ELSEVIER

Eur. J. Mech. B/Fluids 21 (2002) 29–48

EUROPEAN JOURNAL OF MECHANICS B/FLUIDS

Receptivity of boundary layers to three-dimensional disturbances

Sebastian Bake [a,*], Andrey V. Ivanov [b], Hans H. Fernholz [a], Klaus Neemann [a], Yury S. Kachanov [b]

[a] *Hermann-Föttinger-Institut für Strömungsmechanik, Technische Universität Berlin, Strasse des 17. Juni 135, 10623 Berlin, Germany*
[b] *Institute for Theoretical and Applied Mechanics, Russian Academy of Science Siberian Branch 690090 Novosibirsk, Russia*

Abstract

The 3D receptivity of 2D laminar boundary layers to localized surface vibrations has been investigated both experimentally and theoretically for two types of basic flow: (i) the Blasius boundary layer and (ii) a boundary layer with a negative streamwise pressure gradient (Hartree parameter $\beta_H = 0.10$). For the boundary-layer excitation, a specially designed surface vibrator was used. The development of the excited wave-trains was measured by means of hot-wire anemometry and decomposed into oblique normal Tollmien–Schlichting-modes. The initial spectra of the excited perturbations at the position of the vibrator was obtained by two different techniques. The first used an additional source which was mounted upstream and provided the amplification curves for the instability modes in the vicinity of the vibrator, the second was based on linear stability calculations. The receptivity coefficients were defined as the ratio of the initial wavenumber spectrum of the excited TS-waves and the corresponding resonant spectrum of the surface vibrations. They were determined for each fixed frequency as a function of the spanwise wavenumber.

The boundary value problem for the disturbance produced by the vibrating membrane was solved theoretically for the same conditions as in the experiments in the framework of the classical hydrodynamic stability theory. The Navier–Stokes equations were linearized around a incompressible basic flow described by a solution of the Falkner–Skan equation. Comparisons of the theoretical and experimental results on the 3D receptivity show good quantitative agreement. It is concluded that the favorable pressure gradient increases the boundary-layer receptivity to surface vibrations.

Keywords: Receptivity; Surface vibrations; Stability; Boundary layer; Pressure gradient

1. Introduction

Boundary-layer transition starts when instability waves are excited by various external perturbations. This problem is called the ‘receptivity’ of the boundary layer and has a great practical importance for the design of new advanced methods of the transition prediction based on correct physical notions of the mechanisms of excitation of the instability modes by external perturbations of various kinds (such as free-stream vortices, surface roughness and vibrations, acoustic waves, and others). The term ‘receptivity’ was first introduced by Morkovin [1], although a theoretical paper devoted to this problem appeared even earlier (Gaster, [2]). For an overview on the early receptivity investigations see Reshotko [3] and Morkovin [4]. Later results on this topic (70s–80s) were described by Kachanov et al. [5] and Nishioka and Morkovin [6]. Many receptivity mechanisms were considered in a great number of theoretical and experimental studies published in the 1980s and 1990s (see e.g., an overview by Kachanov [7]). In the present paper we will concentrate on the generation of TS-waves by means of unsteady surface non-

* Correspondence and reprints. Present address: Rolls-Royce Deutschland Ltd&CoKG, Eschenweg 11, 15827 Dahlewitz, Germany.
E-mail address: sebastian.bake@rolls-royce.com (S. Bake).

0997-7546/02/$ – see front matter
PII: S0997-7546(01)01156-6

uniformities as one of the possible sources of instability waves in the boundary layer. Most likely, the first theoretical studies of the birth of TS-waves on localized 2D surface vibrations were performed by Terentev [8] and Tumin and Fedorov [9,10]. In the same period similar mechanisms were studied experimentally by Gilev and Kozlov [11]. In particular, it was found that a disturbance source placed at the wall excites 2D TS-waves rather effectively.

Three-dimensional receptivity mechanisms related to surface perturbations in 2D boundary layers were investigated less frequently. The problem of the excitation of 3D TS-waves in 2D boundary layers by surface vibrations has been studied experimentally by Ivanov et al. [12,13] and theoretically by Michalke [14,15] and Michalke and Neemann [16]. A comparison of the experimental and theoretical results of receptivity was performed by Ivanov et al. [17]. Very good qualitative agreement was found, namely, the growth of the receptivity with the growth of frequency of the surface vibrations, and a higher receptivity of the Blasius boundary layer to 3D perturbations than to 2D waves. A quantitative comparison of the receptivity coefficients, however, has shown that the receptivity amplitudes of the experiment were approximately 30% lower than those of the theory. This deviation was most probably caused by the upstream extrapolation of the normal TS-wave amplitudes to the source position.

In the first part of the present work a combined experimental and theoretical study of the linear 3D receptivity of a zero-pressure-gradient (ZPG) boundary layer to localized surface vibrations was carried out followed by a direct quantitative comparison of the receptivity coefficients for various values of spanwise wavenumbers and frequencies. The 2D Blasius-like boundary layer investigated here (for more details see Section 4) developed on the inner wall of a cylindrical test-section of the wind-tunnel with a weak spanwise curvature ($\delta_1/R \approx 0.008$ where δ_1 is the boundary layer displacement thickness and R is the radius of the test-section). It was assumed that the weak wall curvature did not influence the receptivity mechanism. This assumption, however, had to be checked by a comparison of the experimental data with the results of the receptivity calculations performed on a plane wall (see Section 8).

In the second part of the study the same receptivity mechanism was investigated experimentally and theoretically in a flow with a favorable streamwise pressure gradient (FPG case, Hartree parameter $\beta_H = 0.10$). It has been known from the experimental work of Kachanov et al. [18] that an adverse pressure gradient reduces the receptivity to 3D vibrations. This result is in consistence with calculations performed for 2D modes by Michalke and Neemann [19] and for 3D modes by Michalke and Neemann [16] and Neemann [20] for the case of boundary-layer receptivity to periodic blowing or suction on the wall. Quantitative information about the 3D receptivity to surface vibrations in the presence of a favorable pressure gradiend, however, is not available yet.

2. Experimental procedure

2.1. Experimental facility and test model

The experiments were conducted in the Laminar Wind Tunnel of the Hermann-Föttinger-Institute of the Technical University of Berlin. This is a closed-circuit tunnel with an axisymmetric test section made of Plexiglas tubes with an inner diameter of 441 mm and a total length of 6000 mm. The nozzle contraction-ratio was 18 : 1 over a length of 2 m and the boundary layer of the nozzle is blown out. The air was provided by a main radial fan and an additional blower to supply the pressure for removing the nozzle boundary layer. The flow temperature could be controlled by a water cooler and was held constant within $\pm 0.05\,^{\circ}$C. The free-stream turbulence level was below $Tu = 0.05\%$ in the frequency range between 0.1 and 1000 Hz. Measurments with an X-wire in the free-stream showed a ratio of $v'/u' = 0.3$ indicating that the free-stream turbulence consists mainly of volume fluctuations in streamwise direction. (For a more detailed description of the wind-tunnel characteristics see Bake et al. [21].) The boundary layer under investigation developed on the inner wall of the test-section (Fig. 1).

2.2. Disturbance excitation

All measurements were performed at controlled disturbance conditions. Two kinds of disturbance sources were used. The main excitation source (R-source) was a vibrator (Fig. 2) with a circular rubber membrane (of 6 mm diameter and 0.35 mm thickness) flush mounted with the wall at a spanwise position $z = 0$ mm and a streamwise position $x = x_R = 644$ mm downstream of the leading edge (see Fig. 1). The junction between the source membrane and the surface was carefully smoothed to avoid any non-uniformities and to prevent any measurable mean-velocity distortions which could influence the receptivity process.

The second disturbance source (S-source) was a slit source (described in Bake et al. [21]) which worked in a ‘point-source’ regime at a streamwise position $x = x_S = 547$ mm (see Fig. 1). The source was designed to be connected to 32 pipes aligned in spanwise direction but in the ‘point-source’ regime only one pipe was connected to a loudspeaker and the other inlets were closed from outside the wind tunnel. Inside the wind tunnel the slit was kept open. The S-source was used to measure the

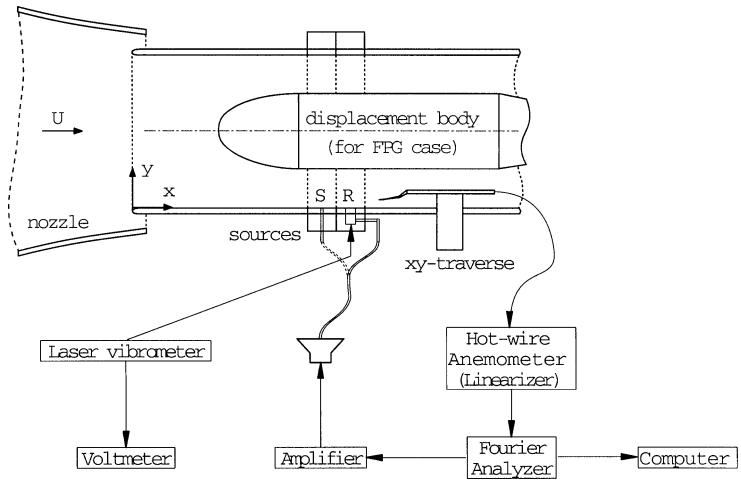

Fig. 1. Sketch of experiment.

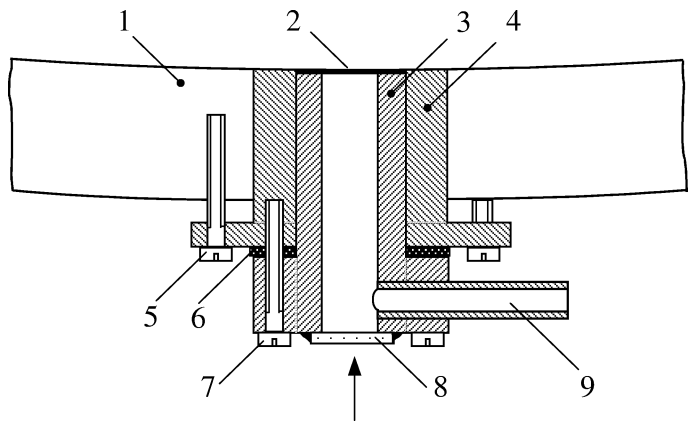

Fig. 2. Sketch of R-source. 1 – test section wall, 2 – rubber membrane, 3 – adjustable source body, 4 – adjustable source holder, 5 – screw to adjust the source holder, 6 – rubber washer, 7 – screw to adjust the source body, 8 – glass window for laser vibrometer, 9 – pipe connected to loudspeaker.

downstream behavior of the 3D normal TS-waves over the whole range of the streamwise coordinate including the position of the R-source.

By means of plastic pipes the sources were connected to the loudspeakers which were exited by harmonic signals produced by an excitation system consisting of a Fourier-Analyzer (Tectronix 2642A) with an output channel and power amplifiers (custom made). The sources were used in sequence and excited the wave trains of time harmonic 3D instability waves.

2.3. Measurements of the vibrator shape

The shape of the vibrator (i.e., the distributions of amplitude and phase of the vibrations in the (x, z)-plane) was measured by means of a laser vibrometer (Polytec OFV 1102) at various amplitudes and frequencies of excitation ensuring linear behavior of the membrane within the range of amplitudes and frequencies used. The characteristics of the membrane oscillations, such as their temperature dependence and axisymmetry, were tested outside the wind tunnel. During the experiments, the dimensional amplitude of the oscillations a_R at the center of the membrane, designated as a_{max}, was kept constant for each frequency tested. The corresponding values are shown in the tables presented in Section 4. The amplitude was controlled permanently during the measurements in the wind-tunnel with the laser vibrometer positioned at the backside (outside the wind tunnel) through a glass window (see Fig. 2). In this way possible changes of the temperature and of the rubber elasticity (degassing of plasticiser) could be taken into account.

In every excitation regime a 'true' value of the phase of vibrations was measured in the center of the source by means of a hot-wire anemometer using the following procedure. The disturbance profile normal to the wall was determined at the position of the R-source center. Then, the phase distribution was extrapolated to the wall by means of a curve fit in the near-wall region using a straight line. While the eigen instability modes excited by the vibrator in its near field have zero amplitudes on the wall, the oscillations produced by the membrane displacements have a maximum on the wall and the phase of this signal is equal to the phase of vibration +180 degrees. When the membrane moves upwards the instantaneous hot-wire signal goes down (and vise versa) because the hot-wire signal is conditioned by the flow displacement in y-direction in the presence of the velocity gradient of the boundary layer.

2.4. Measurements in the flow

All measurements in the flow were conducted with a constant-temperature hot-wire anemometer with linearizer (HDA IIIF, custom made). The gold plated hot wire with 2.5 μm diameter and an effective length of 0.55 mm was mounted on a x, y-traverse. The hot-wire signal was sampled and analyzed by means of a Fourier Analyzer. The disturbance sources could be moved in spanwise direction and were mounted in two metal rings which could be rotated and were inserted between the test section elements. The measurements included spanwise scans of amplitude and phase of the harmonic waves excited by the R-source and S-source separately. For the R-source scans were measured at six x-positions downstream of the source. Similar measurements were performed when the wave-trains were excited by the S-source. The spanwise distributions were measured at this case in the same streamwise positions as for the R-source but an additional distribution was measured at the position of the R-source center ($x = x_R = 644$ mm). The probe distance to the wall was fixed during these measurements. This distance was chosen in order to correspond with the maximum amplitudes of the velocity fluctuations in the TS-waves propagating in the boundary layer (see Section 4 for more detail).

The closest x-position to the R-source was $x - x_R = 50$ mm for the Blasius-case and $x - x_R = 30$ mm for the FPG-case to ensure that the near-field perturbations (consisting of the continuous spectrum modes and bounded fluctuations) had decayed. The distance between the S- and R-source ($\Delta x = 97$ mm) was larger to make sure that the position of the R-source was in the far-field of the S-source. The streamwise length of the near-field was estimated as $\lambda_{xmax}/2$, where λ_{xmax} is the maximum streamwise wavelength of the TS waves studied. Here $\lambda_{xmax}/2$ was 38 mm in the Blasius case and $\lambda_{xmax}/2 \approx 23$ mm in the FPG case.

Due to the symmetry of the disturbance sources and the uniformity of the basic flow the shapes of the wave-trains were also symmetric relative to $z = 0$ mm (see Section 5). This allowed to diminish the measurement errors, resulting for example from very slow temporal mean flow variations, by averaging the left and the right side of the spanwise distributions. Due to small temperatur changes in the laboratory the direction of the mean flow in the axisymetric test-section changed with small angles while measuring a spanwise profile. In the ZPG case the dimensional frequencies of the vibrations were relatively low and they turned out to be rather close to the eigen frequencies of vibrations of the hot-wire probe and the traverse. Due to this, a certain parasitic signal (coherent with the vibrations) was observed in the hot-wire output. To reduce its influence on the measurements a special procedure was used. The amplitude and phase values measured at the frequency of excitation at spanwise positions of the shelfs of the wave train (where the amplitude was constant, e.g., $|z| > 30$ mm in Fig. 7) were averaged as complex numbers and subtracted from the spanwise profiles in the complex plane of the disturbance amplitudes and phases.

2.5. Procedure of experimental data processing

For a fixed oscillations frequency of the R-source the shape of the vibrating membrane in the x, z-plane was subjected to a double Fourier transform. As a result the complex wavenumber spectrum of the vibrations

$$C_{vC}(\alpha_r, \beta) = C_v(\alpha_r, \beta)\, \mathrm{e}^{i\lambda_v(\alpha_r,\beta)} \tag{1}$$

was obtained with the streamwise and spanwise wavenumbers α_r and β, respectively, C_v and λ_v being the real amplitude and the phase of the spectrum. It was found that the shape of the vibrations, normalized by the oscillation amplitude in the vibrator center, was independent of both the frequency and the amplitude in the parameter range used. Therefore, the wavenumber spectrum of the vibrations was universal for all measurement regimes (see Section 7).

The effective input of vibrations to the boundary layer was then found as a 'resonant spectrum of vibrations' by means of the dispersion function $\alpha_r = \alpha_r(\beta)$ for the 3D TS waves which was obtained experimentally at the streamwise position of the R-source $x = x_R = 644$ mm (see Section 6). The resonant spectrum $C_{vC}(\alpha_r(\beta), \beta)$ represents a cut of the two-dimensional spectrum of vibrations along the dispersion curve (see Section 7).

The wave-train of the TS waves excited by the R-source represents the boundary-layer response to the vibrations. For determining the receptivity coefficients an initial spanwise-wavenumber spectrum of the excited TS waves had to be found experimentally at the position of the R-source center. To obtain this information the spanwise distributions of the complex

amplitudes of instability waves measured in the flow were decomposed into normal oblique modes. The procedure of the decomposition was similar to that used by Gilyov et al. [22] and was described in more detail by Kachanov and Michalke [23]. However, the initial wavenumber spectra of the most unstable (discrete-spectrum) TS waves could not be measured directly over the R-source because of the presence of the near-field perturbations associated with the continuous-spectrum modes and bounded fluctuations produced directly by the vibrator. Therefore, the initial spectra were determined by means of an upstream extrapolation of the normal-mode amplitudes and phases measured in the far-field of the R-source. The extrapolation was performed for every normal oblique TS mode separately by means of the corresponding amplification curves obtained in an additional set of measurements by means of the S-source. In the Blasius case, however, the extrapolation was performed by means of theoretical amplification curves because the accuracy of the measurements with the S-source was not high enough. The extrapolation procedure provided the initial complex spanwise wavenumber spectrum of the excited TS waves (that represents the boundary-layer response to the external vibrations)

$$B_{\mathrm{in}C} = B_{\mathrm{in}}(\beta)\,\mathrm{e}^{i\phi_{\mathrm{in}}(\beta)}, \tag{2}$$

where B_{in} and ϕ_{in} are real.

For a fixed value of the disturbance frequency the complex receptivity function $G_{rC}(\beta) = G_r(\beta)\,\mathrm{e}^{i\varphi_r(\beta)}$ (with G_r and φ_r being real) was defined (df) as the ratio

$$G_{rC}(\beta) \stackrel{\mathrm{df}}{=} \frac{B_{\mathrm{in}C}(\beta)}{C_{vC}(\beta)} \tag{3}$$

or separated into amplitude and phase

$$G_r(\beta) \stackrel{\mathrm{df}}{=} \frac{B_{\mathrm{in}}(\beta)}{C_v(\beta)} \quad \text{and} \quad \varphi_r(\beta) \stackrel{\mathrm{df}}{=} \phi_{\mathrm{in}}(\beta) - \lambda_v(\beta). \tag{4}$$

3. Theoretical determination of receptivity coefficients

3.1. Preliminaries

The calculation of stability and receptivity characteristics was performed in the framework of classical hydrodynamic stability theory. The velocity and pressure fields are decomposed into a steady basic flow and an unsteady flow due to the vibrating membrane:

$$\begin{bmatrix} \underline{c}_{\mathrm{all}}(x,y,z,t) \\ p_{\mathrm{all}}(x,y,z,t) \end{bmatrix} = \begin{bmatrix} \underline{C}(x,y,z) \\ P(x,y,z) \end{bmatrix} + \varepsilon \begin{bmatrix} \underline{c}(x,y,z,t) \\ p(x,y,z,t) \end{bmatrix}. \tag{5}$$

The parameter ε, defined as the ratio

$$\varepsilon = \frac{a^*_{\max}}{\delta^*_1} \tag{6}$$

of the maximum amplitude $a^*_{\max}$ of the vibrations and the displacement thickness δ^*_1 of the boundary layer at the streamwise position x^*_{R} of the membrane, is sufficiently small ($\varepsilon \approx 0.05$, see Tables 1 and 2) to allow a linearization of the Navier–Stokes equations around the incompressible basic flow. In addition, the basic flow near the membrane was assumed to be two-dimensional and locally parallel:

$$\underline{C} = U(y)\underline{e}_x, \qquad P = \mathrm{const}, \tag{7}$$

thus neglecting the slow streamwise evolution of the boundary layer and the small velocity component normal to the wall. Since the radius R^* of the axisymmetric test section of the wind tunnel was large compared with the boundary layer thickness ($\delta^*_1/R^* \approx 0.004 \ldots 0.008$), curvature effects were considered to be insignificant which allowed a simplified treatment in a Cartesian frame of reference.

It should be noted that throughout this section, dimensional quantities are marked by a star, whereas symbols without a star refer to nondimensional quantities. The quantities used for nondimensionalization are the constant density ρ^* of the fluid, the displacement thickness δ^*_1 and the velocity U^*_∞ of the outer flow, the latter quantities taken at the position x^*_{R} of the membrane. The Reynolds number Re is defined as $Re = U^*_\infty \delta^*_1/\nu^*$ with ν^* being the constant kinematic viscosity of the fluid.

3.2. Basic flow

The streamwise velocity profile

$$U(y) = f'(\eta) \tag{8}$$

of the basic flow was obtained from solutions of the Falkner–Skan equation of (see, e.g., Schlichting [24])

$$f'''(\eta) + f''(\eta) f(\eta) + \beta_{\mathrm{H}}\big(1 - \big(f'(\eta)\big)^2\big) = 0, \qquad f(0) = f'(0) = 0, \qquad f'(\infty) = 1 \tag{9}$$

after rescaling the similarity variable η to the nondimensional wall distance y:

$$y = \frac{\eta}{I_1}, \quad I_1 = \int_0^\infty \big(1 - f'(\eta)\big)\,\mathrm{d}\eta. \tag{10}$$

The nondimensional pressure gradient or Hartree parameter β_{H} is defined as

$$\beta_{\mathrm{H}} = \frac{2x^*}{U_\infty^*}\frac{\mathrm{d}U_\infty^*}{\mathrm{d}x^*} \tag{11}$$

and was determined from the experimental results as $\beta_{\mathrm{H}} = 0$ for the ZPG case and $\beta_{\mathrm{H}} = 0.1$ for the FPG case, respectively.

3.3. Disturbance flow

The unsteady flow generated by the vibrating membrane is governed by the $\mathrm{O}(\varepsilon)$ terms in the Navier–Stokes equations leading to the following set of linear equations for the velocity components u, v and w (in streamwise, wall-normal and spanwise direction x, y, z respectively) and the pressure p of the disturbance:

$$\frac{\partial u}{\partial x} + \frac{\partial v}{\partial y} + \frac{\partial w}{\partial z} = 0, \tag{12}$$

$$\frac{\partial u}{\partial t} + U\frac{\partial u}{\partial x} + v\frac{\mathrm{d}U}{\mathrm{d}y} = -\frac{\partial p}{\partial x} + \frac{1}{Re}\left(\frac{\partial^2 u}{\partial x^2} + \frac{\partial^2 u}{\partial y^2} + \frac{\partial^2 u}{\partial z^2}\right), \tag{13}$$

$$\frac{\partial v}{\partial t} + U\frac{\partial v}{\partial x} = -\frac{\partial p}{\partial y} + \frac{1}{Re}\left(\frac{\partial^2 v}{\partial x^2} + \frac{\partial^2 v}{\partial y^2} + \frac{\partial^2 v}{\partial z^2}\right), \tag{14}$$

$$\frac{\partial w}{\partial t} + U\frac{\partial w}{\partial x} = -\frac{\partial p}{\partial z} + \frac{1}{Re}\left(\frac{\partial^2 w}{\partial x^2} + \frac{\partial^2 w}{\partial y^2} + \frac{\partial^2 w}{\partial z^2}\right). \tag{15}$$

The disturbance input is represented by inhomogeneous boundary conditions at the position $y = 0$. They result from a linearization of the no-slip condition on the moving surface of the membrane and read in complex notation:

$$u = -\mathrm{D}U(0)h(x,z)\,\mathrm{e}^{-i\omega t}, \qquad v = -i\omega h(x,z)\,\mathrm{e}^{-i\omega t}, \qquad w = 0. \tag{16}$$

The shape of the vibrating membrane, centered around the position $x = x_{\mathrm{R}}$ and $z = 0$, is described by $h(x,z)$, and ω is the (circular) frequency of the vibrations. The symbol $\mathrm{D}(\ldots) = \mathrm{d}(\ldots)/\mathrm{d}y$ is used to denote differentiation with respect to y. Far away from the wall the disturbances are required to vanish:

$$u, v, w, p \to 0 \quad \text{for } y \to \infty. \tag{17}$$

Assuming appropriate boundedness conditions, Eqs. (12)–(15) can be solved by means of a combined Fourier–Laplace transform with respect to t, x and z, respectively; thereby introducing the wavenumbers α and β and the complex frequency s:

$$\begin{bmatrix} \tilde{\underline{c}}(\alpha, y, \beta, s) \\ \tilde{p}(\alpha, y, \beta, s) \end{bmatrix} = \int_0^{+\infty} \mathrm{d}t\,\mathrm{e}^{ist} \int_{-\infty}^{+\infty} \mathrm{d}x\,\mathrm{e}^{-i\alpha x} \int_{-\infty}^{+\infty} \mathrm{d}z\,\mathrm{e}^{-i\beta x} \begin{bmatrix} \underline{c}(x, y, z, t) \\ p(x, y, z, t) \end{bmatrix}. \tag{18}$$

As a result, the governing equations are transformed into a set of ordinary differential equations equivalent to the three-dimensional Orr–Sommerfeld and Squire equations:

$$\mathrm{D}\tilde{v} = -i\alpha\tilde{u} - i\beta\tilde{w}, \tag{19}$$

$$\mathrm{D}^2\tilde{u} = Re\,\mathrm{D}U\tilde{v} + \big(\alpha^2 + \beta^2 - iRe(s - \alpha U)\big)\tilde{u} + i\alpha Re\,\tilde{p}, \tag{20}$$

$$\mathrm{D}\tilde{p} = -\frac{1}{Re}\big(\alpha^2+\beta^2 - iRe(s-\alpha U)\big)\tilde{v} - \frac{i\alpha}{Re}\mathrm{D}\tilde{u} - \frac{i\beta}{Re}\mathrm{D}\tilde{w}, \tag{21}$$

$$\mathrm{D}^2\tilde{w} = \big(\alpha^2+\beta^2 - iRe(s-\alpha U)\big)\tilde{w} + i\beta Re\,\tilde{p}. \tag{22}$$

The boundary conditions are:

$$\tilde{u} = -\mathrm{D}U(0)\tilde{h}\frac{i}{s-\omega}, \qquad \tilde{v} = -i\omega\tilde{h}\frac{i}{s-\omega}, \qquad \tilde{w} = 0 \quad \text{at } y = 0, \tag{23}$$

with $\tilde{h} = \tilde{h}(\alpha,\beta)$ being the two-dimensional Fourier transform (equivalent to C_{vC} in Section 2) of the shape function $h(x,z)$, and

$$\tilde{u},\tilde{v},\tilde{w},\tilde{p} \to 0 \quad \text{for } y \to \infty. \tag{24}$$

In general, Eqs. (19)–(22) have to be solved numerically, but at large distances from the wall $y \gg 1$ (due to $U(y) \to 1, \mathrm{D}U(y) \to 0$ for $y \to \infty$), their six fundamental solutions can be written in terms of exponentials:

$$\begin{bmatrix}\tilde{u}\\ \tilde{v}\\ \tilde{w}\\ \tilde{p}\end{bmatrix}_{(1,2,3,4,5,6)} \to \begin{bmatrix}\mp i\zeta\\ \alpha+\beta\\ \mp i\zeta\\ 0\end{bmatrix}\mathrm{e}^{\mp\zeta y}, \begin{bmatrix}\mp i\zeta\\ \alpha-\beta\\ \pm i\zeta\\ 0\end{bmatrix}\mathrm{e}^{\mp\zeta y}, \begin{bmatrix}\mp i\alpha/\sigma\\ 1\\ \mp i\beta/\sigma\\ \mp i(s-\alpha)/\sigma\end{bmatrix}\mathrm{e}^{\mp\sigma y}, \tag{25}$$

with:

$$\zeta = \sqrt{\alpha^2+\beta^2 - iRe(s-\alpha)}, \qquad \sigma = \sqrt{\alpha^2+\beta^2}. \tag{26}$$

The exponentially growing solutions $\mathrm{e}^{+\zeta y}$ and $\mathrm{e}^{+\sigma y}$, denoted by even indices, are ruled out by the condition (24), so that the solution of the boundary value problem can be written as:

$$\begin{bmatrix}\tilde{\underline{c}}\\ \tilde{p}\end{bmatrix} = k_1\begin{bmatrix}\tilde{\underline{c}}_1\\ \tilde{p}_1\end{bmatrix} + k_3\begin{bmatrix}\tilde{\underline{c}}_3\\ \tilde{p}_3\end{bmatrix} + k_5\begin{bmatrix}\tilde{\underline{c}}_5\\ \tilde{p}_5\end{bmatrix}. \tag{27}$$

The constants k_1, k_3 and k_5 have to be determined from the boundary conditions (23) which yield after some linear algebra:

$$\begin{bmatrix}\tilde{\underline{c}}\\ \tilde{p}\end{bmatrix} = \frac{i\tilde{h}}{(s-\omega)\Delta}\Bigg(-\mathrm{D}U(0)\Bigg(\Delta_{u1}\begin{bmatrix}\tilde{\underline{c}}_1\\ \tilde{p}_1\end{bmatrix} + \Delta_{u3}\begin{bmatrix}\tilde{\underline{c}}_3\\ \tilde{p}_3\end{bmatrix} + \Delta_{u5}\begin{bmatrix}\tilde{\underline{c}}_5\\ \tilde{p}_5\end{bmatrix}\Bigg) - i\omega\Bigg(\Delta_{v1}\begin{bmatrix}\tilde{\underline{c}}_1\\ \tilde{p}_1\end{bmatrix} + \Delta_{v3}\begin{bmatrix}\tilde{\underline{c}}_3\\ \tilde{p}_3\end{bmatrix} + \Delta_{v5}\begin{bmatrix}\tilde{\underline{c}}_5\\ \tilde{p}_5\end{bmatrix}\Bigg)\Bigg), \tag{28}$$

with:

$$\begin{aligned}
\Delta_{u1} &= +\begin{vmatrix}\tilde{v}_3 & \tilde{v}_5\\ \tilde{w}_3 & \tilde{w}_5\end{vmatrix}_{y=0}, \qquad \Delta_{u3} = -\begin{vmatrix}\tilde{v}_1 & \tilde{v}_5\\ \tilde{w}_1 & \tilde{w}_5\end{vmatrix}_{y=0}, \qquad \Delta_{u5} = +\begin{vmatrix}\tilde{v}_1 & \tilde{v}_3\\ \tilde{w}_1 & \tilde{w}_3\end{vmatrix}_{y=0},\\
\Delta_{v1} &= -\begin{vmatrix}\tilde{u}_3 & \tilde{u}_5\\ \tilde{w}_3 & \tilde{w}_5\end{vmatrix}_{y=0}, \qquad \Delta_{v3} = +\begin{vmatrix}\tilde{u}_1 & \tilde{u}_5\\ \tilde{w}_1 & \tilde{w}_5\end{vmatrix}_{y=0}, \qquad \Delta_{v5} = -\begin{vmatrix}\tilde{u}_1 & \tilde{u}_3\\ \tilde{w}_1 & \tilde{w}_3\end{vmatrix}_{y=0},
\end{aligned} \tag{29}$$

and:

$$\Delta = \begin{vmatrix}\tilde{u}_1 & \tilde{u}_3 & \tilde{u}_5\\ \tilde{v}_1 & \tilde{v}_3 & \tilde{v}_5\\ \tilde{w}_1 & \tilde{w}_3 & \tilde{w}_5\end{vmatrix}_{y=0}. \tag{30}$$

The determinant Δ is a function of the Fourier–Laplace transform variables. Its zeros are the eigenvalues of the homogeneous stability problem, i.e. $\Delta(\alpha,\beta,s) = 0$ constitutes the dispersion relation of the instability waves.

The integration contours $C(s)$, $C(\alpha)$ and $C(\beta)$ for the inverse Fourier–Laplace transform

$$\begin{bmatrix}\underline{c}(x,y,z,t)\\ p(x,y,z,t)\end{bmatrix} = \frac{1}{8\pi^3}\int_{C(s)}\mathrm{d}s\,\mathrm{e}^{-ist}\int_{C(\alpha)}\mathrm{d}\alpha\,\mathrm{e}^{i\alpha x}\int_{C(\beta)}\mathrm{d}\beta\,\mathrm{e}^{i\beta x}\begin{bmatrix}\tilde{\underline{c}}(\alpha,y,\beta,s)\\ \tilde{p}(\alpha,y,\beta,s)\end{bmatrix} \tag{31}$$

are determined by the poles of the integrand in Eq. (28). Valid choices are the real α- and β-axes and a line above the highest temporal mode of $\Delta(\alpha,\beta,s) = 0$ (for given real values of α and β) in the s-plane (see upper part of Fig. 3). For convectively

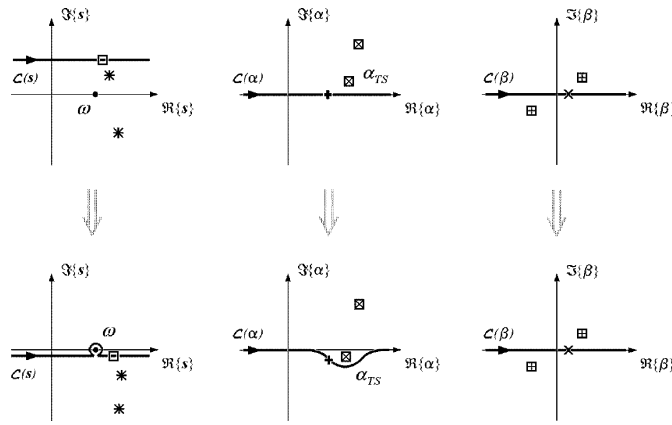

Fig. 3. Integration contours and solutions of the dispersion relation in the complex s-, α- and β-planes. The points on two of the integration contours are mapped by $\Delta(\alpha, \beta, s) = 0$ onto the points marked by the same symbols in the third plane.

unstable flows, however, the integration contours can be deformed to a more suitable position shown in the lower part of Fig. 3 (see, e.g., Ashpis and Reshotko [26]). In this configuration it can be seen that the behaviour for large times t after switching on the vibrations is determined by the pole $s = \omega$, whereas the solution at large distances $x - x_s$ downstream of the membrane is dominated by the pole $\alpha = \alpha_{\mathrm{TS}}(\beta, \omega)$ which has moved from the upper into the lower α-halfplane $\Im\{\alpha\} < 0$. The remaining part of $C(\alpha)$ along the real α-axis is responsible for the disturbance field near the membrane. It has been shown numerically (Michalke and Neemann [19]) and experimentally (Gilev and Kozlov [11]) that the near field decays rapidly both in upstream and downstream directions. Therefore, the spatial mode associated with α_{TS} is also considered to be the dominant part of the solution, if the imaginary part $\Im\{\alpha_{\mathrm{TS}}\}$ is actually positive, but changes its sign for different parameters ω, β, β_{H} and *Re*.

The dominant part of the solution is closely related to the Tollmien–Schlichting waves known from viscous stability theory. Since $\alpha_{\mathrm{TS}}(\beta, \omega)$ satisfies the dispersion relation $\Delta(\alpha_{\mathrm{TS}}, \beta, \omega) = 0$ for given frequency ω and spanwise wavenumber β, the subdeterminants in Eq. (29) are not independent from each other, but are related by $\Delta_{u1} = \Delta_{v1}\Delta_{u5}/\Delta_{v5}$ and $\Delta_{u3} = \Delta_{v3}\Delta_{u5}/\Delta_{v5}$, for example. If the eigenfunctions of the stability problem are defined as

$$\begin{bmatrix} \underline{\tilde{c}}_e \\ \tilde{p}_e \end{bmatrix} = \Delta_{v1} \begin{bmatrix} \underline{\tilde{c}}_1 \\ \tilde{p}_1 \end{bmatrix} + \Delta_{v3} \begin{bmatrix} \underline{\tilde{c}}_3 \\ \tilde{p}_3 \end{bmatrix} + \Delta_{v5} \begin{bmatrix} \underline{\tilde{c}}_5 \\ \tilde{p}_5 \end{bmatrix}, \tag{32}$$

the dispersion relation can be recast into:

$$\Delta(\alpha, \beta, s) = \tilde{v}_e(\alpha, y = 0, \beta, s) = 0. \tag{33}$$

Application of the residue theorem from complex analysis to Eq. (31) then yields for a single spanwise mode of the dominant part:

$$\begin{bmatrix} \underline{c}(x, y, z, t) \\ p(x, y, z, t) \end{bmatrix}_{\mathrm{TS}} = \underbrace{\tilde{h}(\alpha_{\mathrm{TS}}, \beta)}_{\text{(a)}} \underbrace{\frac{\omega - i\mathrm{D}U(0)\Delta_{u5}/\Delta_{v5}}{\frac{\partial \tilde{v}_e(\alpha, y=0, \beta, \omega)}{\partial \alpha}\big|_{\alpha=\alpha_{\mathrm{TS}}}} \begin{bmatrix} \tilde{\underline{c}}_e(\alpha_{\mathrm{TS}}, y, \beta, \omega) \\ p_e(\alpha_{\mathrm{TS}}, y, \beta, \omega) \end{bmatrix}}_{\text{(b)}} \underbrace{\mathrm{e}^{i(\alpha_{\mathrm{TS}}(x - x_{\mathrm{R}}) + \beta z - \omega t)}}_{\text{(c)}}. \tag{34}$$

The complete dominant part is not needed in the present investigation, but can be obtained by an integration over all spanwise wavenumbers β leading to eigenvalues $\alpha_{\mathrm{TS}}(\beta, \omega)$ with $\Im\{\alpha_{\mathrm{TS}}\} < 0$ (see Michalke and Neemann [16]).

The second term (b) in Eq. (34) couples the Fourier spectrum of the membrane (a) with the wave term (c) and can be interpreted in two ways: (1) as a transfer function between the membrane vibrations and the wave motion downstream of the membrane, or (2) as a complex initial amplitude, normalized by the input spectrum $\tilde{h}(\alpha_{\mathrm{TS}}, \beta)$, of the Tollmien–Schlichting wave at the source position $x = x_{\mathrm{R}},\ z = 0$. In an experimental investigation it is simple to determine the u-component of term (b) which is therefore defined as the receptivity coefficient

$$G(y, \beta, \omega) = \frac{\omega - i\mathrm{D}U(0)\Delta_{u5}/\Delta_{v5}}{\frac{\partial \tilde{v}_e(\alpha, y=0, \beta, \omega)}{\partial \alpha}\big|_{\alpha=\alpha_{\mathrm{TS}}}} \tilde{u}_e(\alpha_{\mathrm{TS}}, y, \beta, \omega). \tag{35}$$

The receptivity coefficient G still depends on the wall distance y, but is conveniently evaluated at a position near the maximum of $|\tilde{u}_e|$, then called G_{rC} according to Section 2.

3.4. Numerical procedures

Eqs. (19)–(22) were solved numerically by means of a Runge–Kutta–Fehlberg procedure of 8th order combined with an extended version of the reduction method originally developed by van Stijn and van de Vooren [25] (see Neemann [20] for more details). In order to find the eigenvalues α_{TS} of the spatial stability problem, a zero search procedure of the Muller type was used, and the derivative in Eq. (35) was approximated by central differences.

4. Mean-flow characteristics and parameters of the experiments

4.1. Blasius boundary layer

It is necessary to note, that because the wind-tunnel test-section has a constant diameter, the downstream growth of the boundary layer thickness provides a very weak flow acceleration in the test-section. Nevertheless, the mean flow in this case was very close to the theoretical Blasius solution (Fig. 4). Indeed, the shape factor H_{12}, calculated from the experimental data, was equal to 2.58 (Blasius: $H_{12} = 2.59$). The Reynolds number Re (based on the boundary layer displacement thickness δ_{1R}) is shown in Table 1. The displacement thickness δ_{1R}, the flow velocity U_{0R}, and the Reynolds number were determined at the position of the R-source.

The dimensional frequencies of the vibrations and the corresponding frequency parameters are also shown in Table 1 together with the dimensional amplitudes of vibration a_{max} measured at the center of the R-source. (The shape of vibrations is described in Section 7.)

Note, that in all measurement regimes (for the two disturbance sources) the amplitudes of the excitation were chosen small enough to provide linearity of both the stability and receptivity mechanisms. This was checked by measurements of several wall-normal and spanwise distributions of the disturbance amplitudes and phases at two or three different amplitudes of excitation. In the main measurement regimes only those levels of excitation were used which showed no influence of the excitation amplitude on the shape of the excited wave-train.

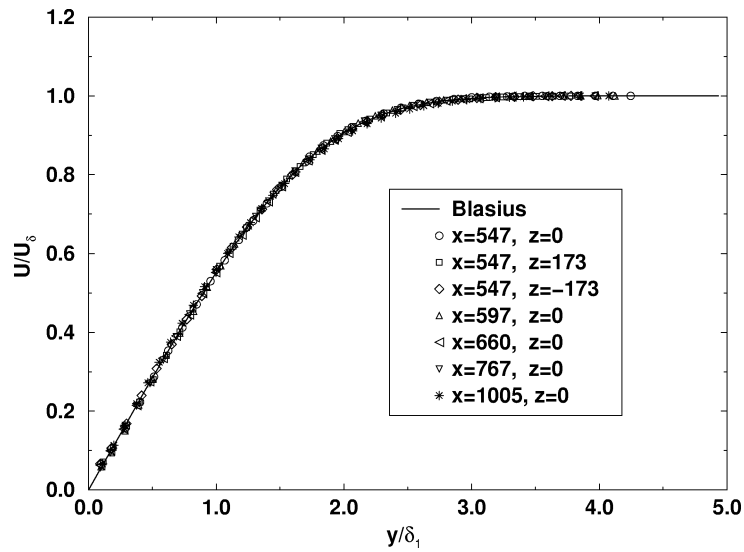

Fig. 4. Mean velocity profiles measured in the ZPG case at different streamwise and spanwise positions (in mm) in comparison with the theoretical Blasius profile.

Table 1
Experimental parameters for the Blasius case

U_{0R} [m/s]	δ_{1R} [mm]	Re	f [Hz]	$F \times 10^6$	a_{max} [mm]
7.5	1.91	946	37.75	64.4	0.057
7.5	1.91	946	55.75	94.9	0.072
7.5	1.91	946	75.00	127.6	0.091

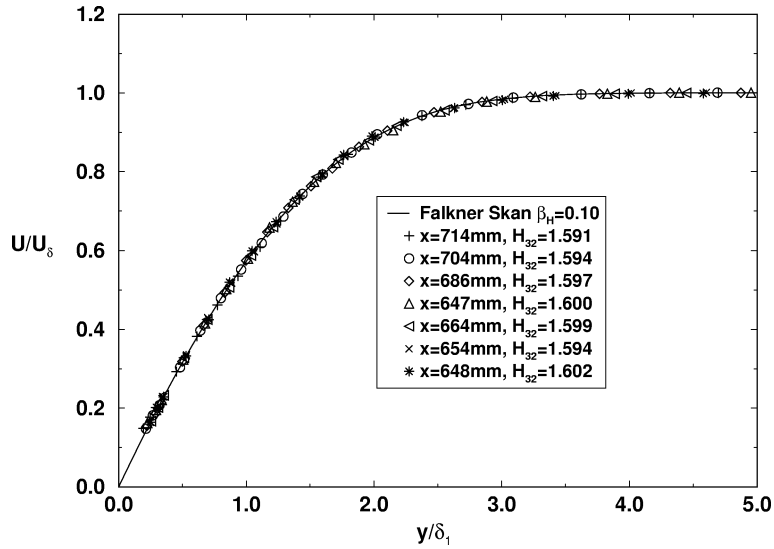

Fig. 5. Mean velocity profiles measured in the FPG case at different streamwise positions in comparison with the theoretical Falkner–Skan profile ($\beta_H = 0.10$).

Table 2
Experimental parameters for the FPG case

U_{0R} [m/s]	δ_{1R} [mm]	Re	f [Hz]	$F \times 10^6$	a_{max} [mm]
12.4	0.87	698	103.1	65.1	0.056
12.4	0.87	698	152.5	97.8	0.041
12.4	0.87	698	205.0	130.7	0.033

The positions of the measurements in the (F, Re)-plane ($F = 2\pi f \nu / U_\infty^2$) with respect to the calculated neutral stability curves for 2D TS waves are shown in Fig. 6 for both ZPG and FPG cases.

4.2. Boundary layer with favorable pressure gradient

In order to provide a favorable pressure gradient corresponding to a laminar boundary layer with a Hartree parameter of $\beta_H = 0.10$ an axisymmetric displacement body described by Fernholz and Warnack [27] was used (see Fig. 1). The Hartree parameter was determined by measuring the free-stream velocity U_∞ along a streamwise line above the boundary layer and fitting it to a function $U_\infty \sim x^m$, where $m = \beta_H/(2 - \beta_H)$. The deviation between the experimental and the theoretical shape factor $H_{32} = \delta_3/\delta_2 = 1.597$ was less than 0.4% (where δ_2 and δ_3 are the boundary layer momentum loss thickness and energy thickness, respectively).

The mean-velocity profiles show good qualitative agreement with the theoretical Falkner–Skan profile (Fig. 5) calculated for $\beta_H = 0.1$. Because of the growth of the background disturbance level in the wind tunnel at higher free-stream velocities, it was not possible to provide the same value of the Reynolds number in the FPG and in the Blasius case. The slightly lower Reynolds number was accepted because the experimental results can be compared with theoretical ones at the same Reynolds number, and the influence of the Reynolds number can be shown by theory alone. The boundary layer and frequency parameters for the experiments in the FPG case are shown in Table 2. The dimensional disturbance frequencies were changed to obtain the same values of the frequency parameter $F = 2\pi f \nu / U_0^2$ in both boundary layers.

5. Downstream evolution of the wave trains

In order to reduce the size of the paper (and because of the qualitatively similar behavior of the perturbations in different regimes) only the results obtained in one of the six measured regimes are presented in Sections 5 and 6. In this regime the frequency of the perturbations was $f = 152.5$ Hz (the medium frequency) and the pressure gradient was favorable. However, the final results of the receptivity study are presented in section 8 for all regimes investigated experimentally and theoretically.

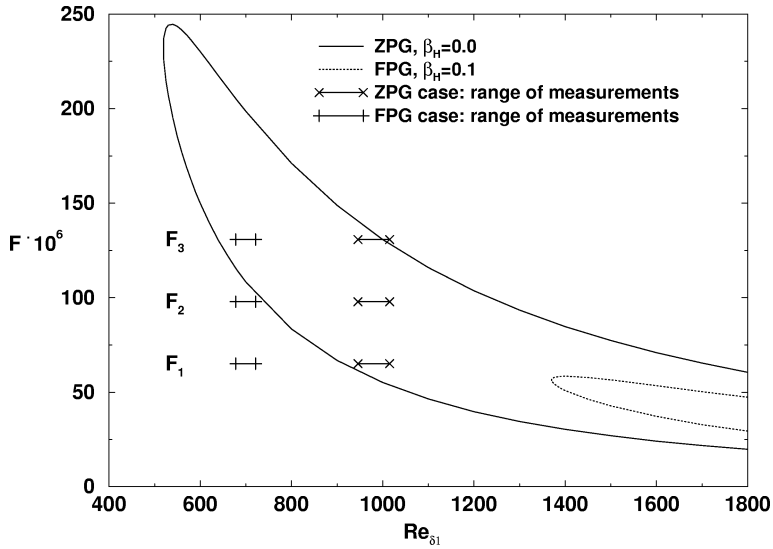

Fig. 6. Neutral stability curves for 2D TS waves and ranges of measurements for the ZPG and the FPG case.

5.1. Normal-to-wall profiles

The normal-to-wall profiles of the mean flow velocity and the disturbance amplitudes and phases were measured in all regimes at various spanwise and streamwise positions. These measurements were aimed at finding the non-dimensional distance from the wall that would be closest to the amplitude maxima for all 3D TS-modes under investigation. This distance can be chosen, however, as a compromise between the exact positions of the amplitude maxima which are different for the TS waves inclined at different angles to the flow direction. In the ZPG case the 'optimal' distance was determined as $y/\delta_1 = 0.77$ ($U/U_0 = 0.435$). This result agrees with previous observations in the Blasius flow (see, e.g., Ivanov, Kachanov and Obolentseva [13]). In the FPG case the distance chosen was $y/\delta_1 = 0.85$ ($U/U_0 = 0.490$). Subsequent calculations have shown that these distances are indeed rather close to the position of the amplitude maxima of normal 3D TS waves and represent a reasonable compromise.

In every measurement regime the profiles of the mean flow velocity and the disturbance amplitudes and phases were also measured at the position of the R-source center to obtain the phase value of the membrane vibration (see Section 2).

5.2. Spanwise distributions

The evolution of the wave trains downstream of the membrane (the R-source) was measured at six x-positions, and the wall-normal distances which corresponded approximately to the amplitude maxima of the normal TS modes are shown in Fig. 7 for the frequency ($f = 152.5$ Hz) in the FPG case.

When the R-source was switched off and only the S-source was used, another set of the spanwise profiles was measured at the same streamwise positions and, in addition, at the position of the R-source center ($x = 644$ mm, $\Delta x = 0$ mm). An example of this set is shown in Fig. 8 for the same frequency and for the FPG case. Similar to the case of the R-source (Fig. 7), the S-source excites a very symmetric wavetrain that remains symmetric downstream in the whole range of the streamwise coordinates. It is seen that the shapes of the spanwise distributions measured for the S-source are quite different from those obtained for the R-source because the initial spectra of the excited waves are different. However, the behavior of normal TS-modes is governed completely by the boundary-layer stability and independent of the initial spectrum, providing information about the normal-mode amplification curves (see below).

6. Evolution of normal instability modes

6.1. Spanwise wavenumber spectra

In order to obtain information about the generation and spatial development of the normal oblique TS modes, the spanwise distributions of the disturbance amplitude and phase, like those shown in Figs. 7 and 8, were subjected to a spatial Fourier

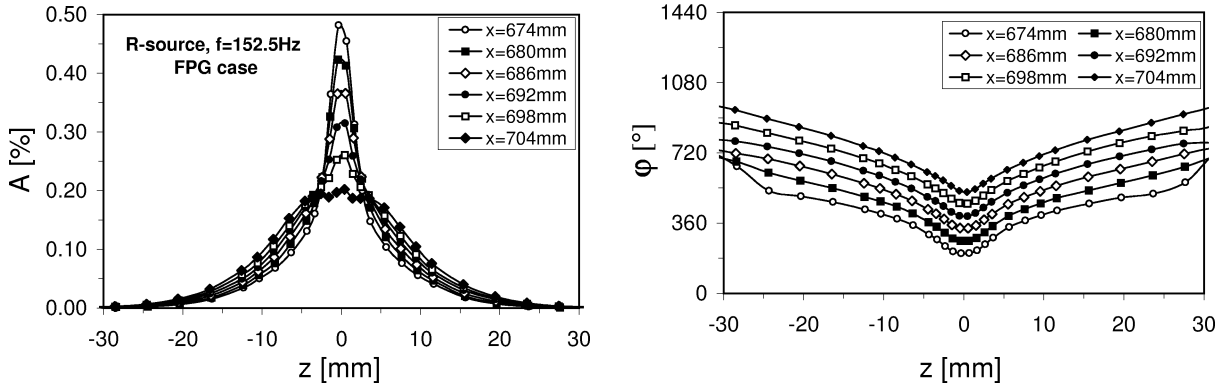

Fig. 7. Spanwise profiles downstream of the R-source: amplitude [left] and phase [right] at different x-positions and $f = 152.5$ Hz in the FPG case.

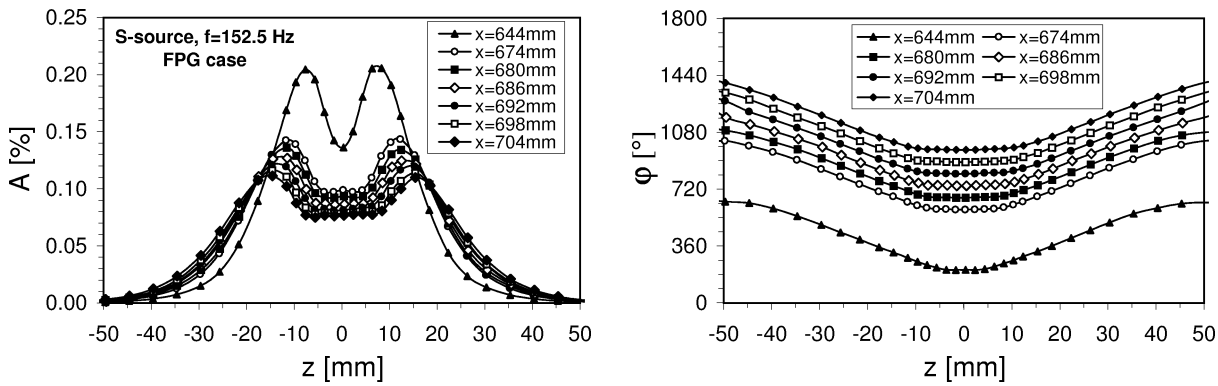

Fig. 8. Spanwise profiles downstream of the S-source: amplitude [left] and phase [right] at different x-positions and $f = 152.5$ Hz in the FPG case.

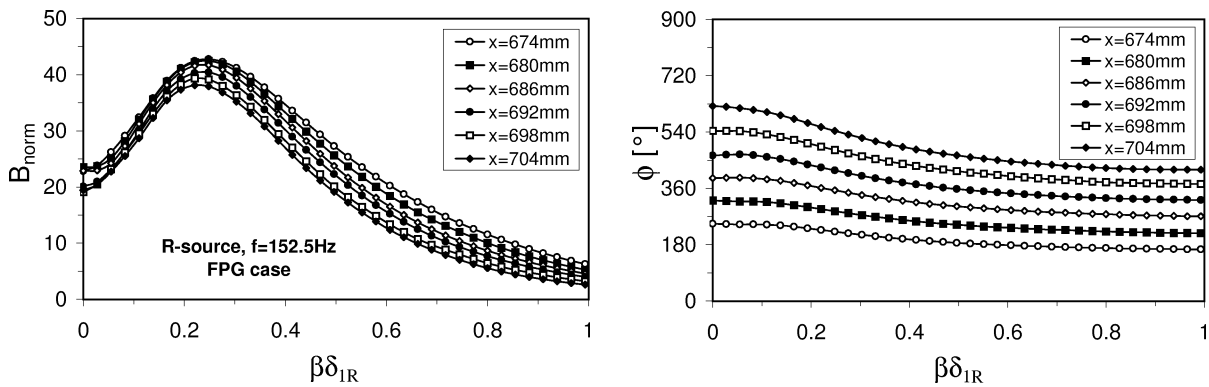

Fig. 9. Spanwise wavenumber spectra of the wave-train excited by the R-source: amplitude [left] and phase [right] at different x-positions and $f = 152.5$ Hz in the FPG case.

transform. As a result, the spanwise wavenumber spectra of the perturbations were obtained. Two sets of these spectra for the FPG case are shown in Fig. 9 for the R-source and in Fig. 10 for the S-source. The wavenumber β was normalized by the boundary-layer displacement thickness δ_{1R} measured at the position of the R-source center and the TS-wave amplitude B is shown in percent of the potential flow velocity over the R-source normalized by the maximum amplitude $a_R(x_R, z = 0)$ of the membrane. Because of the symmetry of the spanwise distributions only one half of the spanwise wavenumber spectra is shown in Figs. 9 and 10. Due to the influence of the favorable pressure gradient the amplitudes of all normal TS waves decrease. The phases of these modes increase, however, showing travelling waves propagating downstream.

6.2. Initial wavenumber spectra

The spanwise wavenumber spectra as those shown in Figs. 9 and 10 allowed us to obtain the streamwise distributions of the normal TS-mode amplitudes and phases for every fixed value of the spanwise wavenumber. These distributions were used for determining the initial spanwise wavenumber spectra of perturbations induced by the R-source. The procedure how to determine the initial normal TS-mode amplitudes and phases is illustrated in Fig. 11 for the ZPG case and in Fig. 12 for the

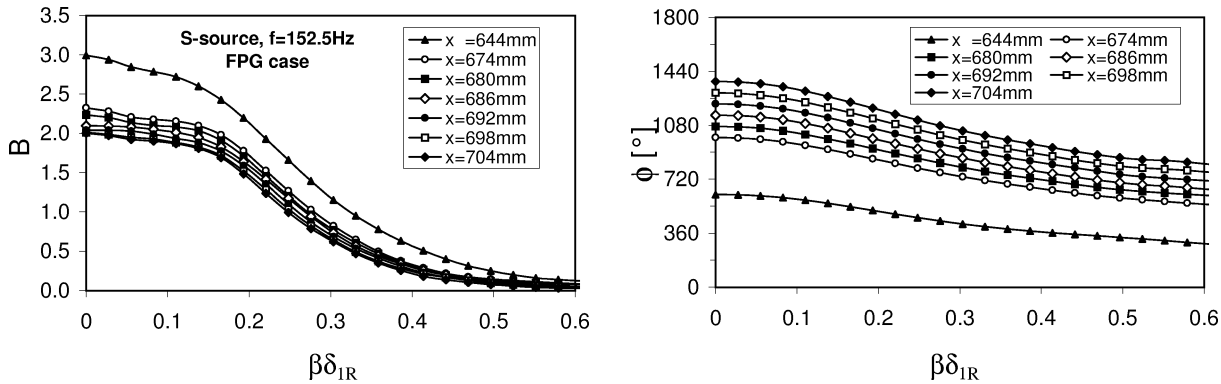

Fig. 10. Spanwise wavenumber spectra of the wave-train excited by the S-source: amplitude [left] and phase [right] at different x-positions and $f = 152.5$ Hz in the FPG case.

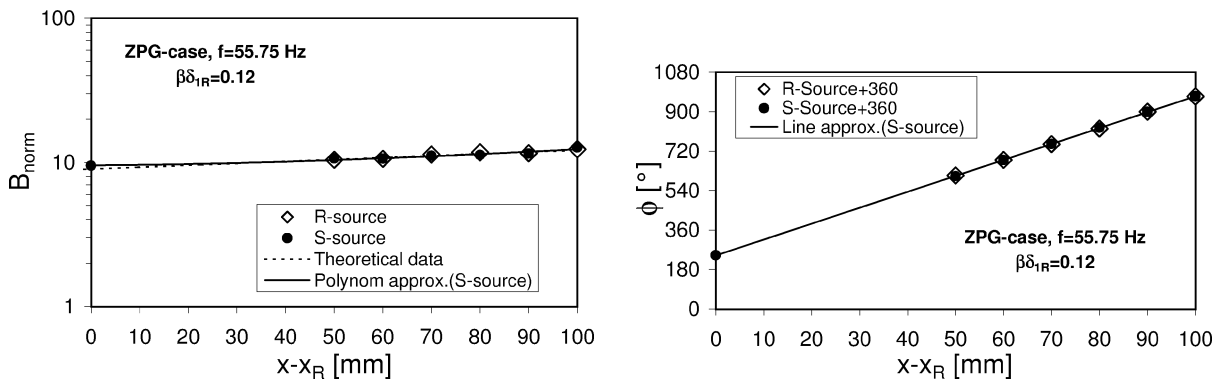

Fig. 11. Procedure of extrapolation of the normal TS-wave amplitude [left] and phase [right] to the R-source center (at $x - x_R = 0$) for the ZPG case. $f = 55.75$ Hz, $\beta\delta_{1R} = 0.12$.

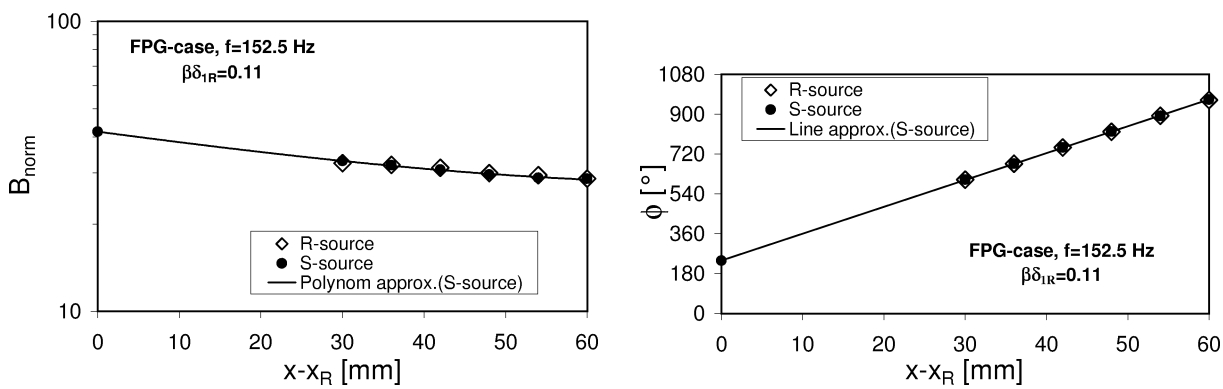

Fig. 12. Procedure of extrapolation of the normal TS-wave amplitude [left] and phase [right] to the R-source center (at $x - x_R = 0$) for the FPG case. $f = 152.5$ Hz, $\beta\delta_{1R} = 0.11$.

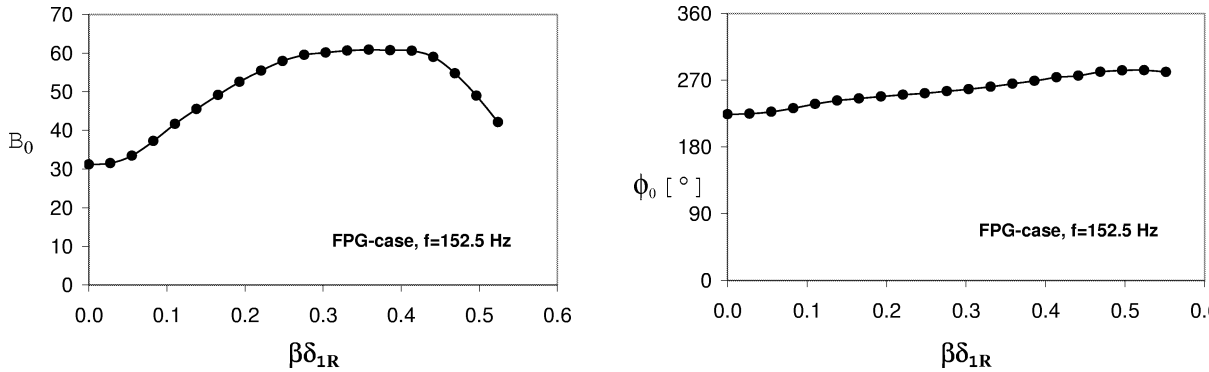

Fig. 13. Amplitude [left] and phase [right] parts of the initial spanwise wavenumber spectrum of TS-waves determined at the position of the R-source for the FPG case and $f = 152.5$ Hz.

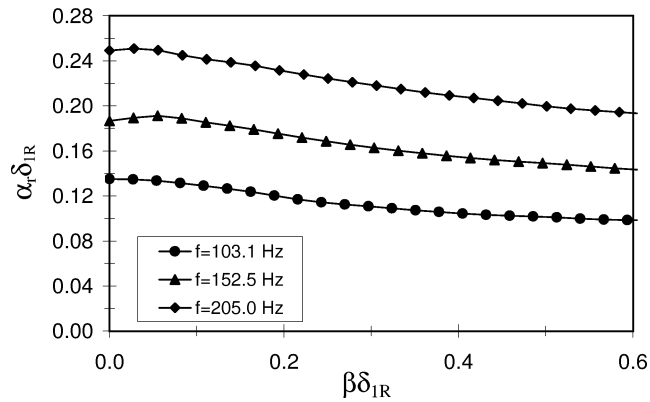

Fig. 14. Initial dispersion functions measured for three disturbance frequencies in the FPG case.

FPG case for one of the normal TS waves. For the R-source the spectral amplitudes were normalised by the amplitude of the membrane vibration measured in its center. The open symbols represent the spectral amplitudes and phases of normal instability modes (with $\beta\delta_{1R} = 0.120$ in Fig. 11 and $\beta\delta_{1R} = 0.110$ in Fig. 12) generated by the R-source. The closed symbols show the corresponding data obtained for the same modes for the S-source. The S-source amplitudes are multiplied by a certain factor in order to match them with the R-source amplitudes, while the S-source phases are shifted by a certain value in order to match them with the R-source phases. The closed symbols at $x - x_R = 0$ give the initial amplitudes and phases of the given normal modes. This procedure was applied to every normal mode in every regime of the measurements.

An example of the initial spanwise wavenumber spectrum is shown in Fig. 13 for the FPG case for the vibration frequency $f = 152.5$ Hz. This spectrum (as well as the similar spectra obtained in other regimes) was used for determining the receptivity coefficients.

6.3. Initial dispersion curves

The streamwise distributions of the normal TS-mode phases (like those shown in Fig. 12 (right) and Fig. 11 (right)) were used to determine the dispersion functions of the 3D TS-wave $\alpha_R = \alpha_R(\beta, f)$ at the position of the R-source center (see also Kachanov and Michalke [23]). It was found that in both the FPG- and the ZPG-case the streamwise phase distributions could be approximated very well by straight lines. This means that the dimensional streamwise wavenumber, $\alpha_R = \tan(\phi)$, is independent of the streamwise coordinate x. For every fixed disturbance frequency the initial non-dimensional dispersion curve $\alpha_R\delta_{1R} = \alpha_R\delta_{1R}(\beta\delta_{1R})$ was found as a product of the dimensional α_R (determined for every given value of the spanwise wavenumber β) and the boundary-layer displacement thickness δ_{1R}.

The dispersion functions obtained experimentally in the FPG case are shown in Fig. 14 for the three frequencies studied. Qualitatively they are very similar to those measured in the ZPG case (see also Ivanov et al. [13]). According to the procedure of processing the experimental data the initial dispersion functions were used for the selection of the resonant modes of the 2D wavenumber spectrum of the R-source vibrations and for the determination the receptivity functions (see section 8). In

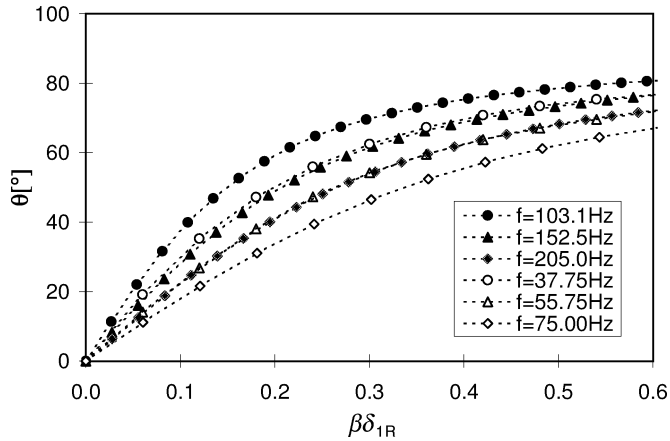

Fig. 15. Experimental values of the wave propagation angle versus spanwise wavenumber determined at the R-source position.

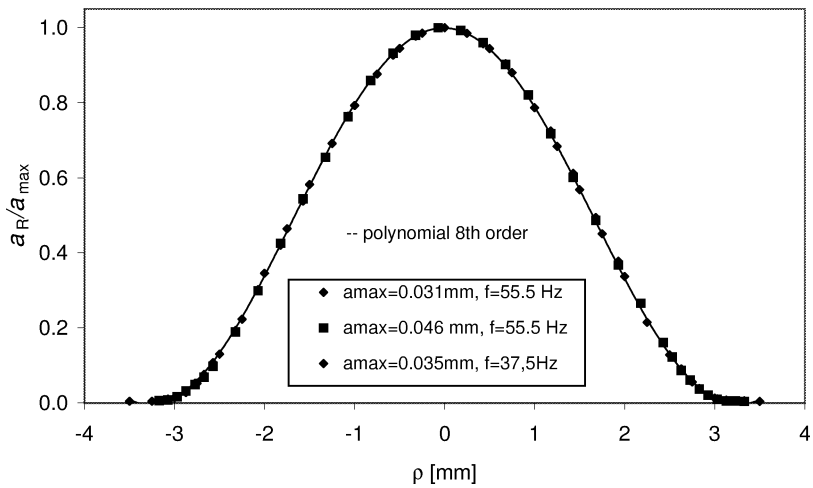

Fig. 16. Distribution of the membrane oscillation amplitude, normalized by the amplitude in its center, along the R-source diameter at three amplitudes of excitation and two frequencies together with a polynomial approximation.

agreement with previous studies the dependence of the streamwise wavenumber α_R on the spanwise wavenumber β is a unique function for every fixed frequency. The wave propagation angle θ can be easily found for every value of β as $\theta = \tan^{-1}(\beta/\alpha_R)$. The corresponding values of θ are shown in Fig. 15 for all regimes studied.

7. Analysis of the shape of vibrations

7.1. Shape of the vibrator in physical space

Some measured amplitudes of the membrane oscillations (normalized by the maximum in the membrane center) are shown in Fig. 16 as a function of the distance ρ from the R-source center. The phase of the R-source oscillations turned out to be constant across the membrane (not shown). The shape of the oscillation distribution is axisymmetric. This shape was also independent of both amplitude and frequency in the range of parameters used in the main regimes of the measurements. This is illustrated in Fig. 16 for two amplitudes and two excitation frequencies. The spatial distribution of the membrane oscillations, normalized by the amplitude in its center, is presented in Fig. 17. The axisymmetric shape of the R-source oscillations together with the constant oscillation phase allowed a simplified description of the membrane oscillations, since only the radial distribution of the amplitudes (as that shown in Fig. 16) has to be known. For this purpose the experimental data points in Fig. 16 were

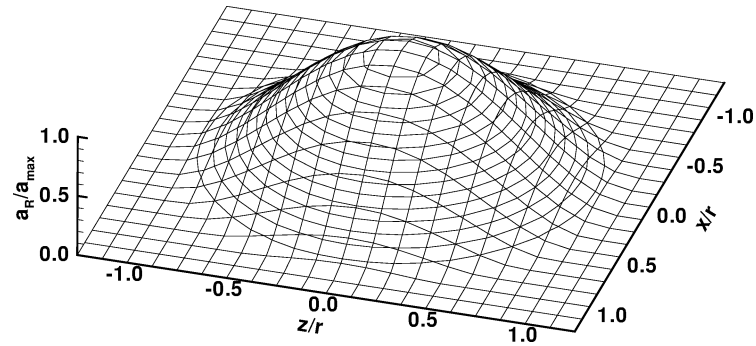

Fig. 17. Spatial distribution of the membrane oscillation amplitude normalized by the amplitude in its center.

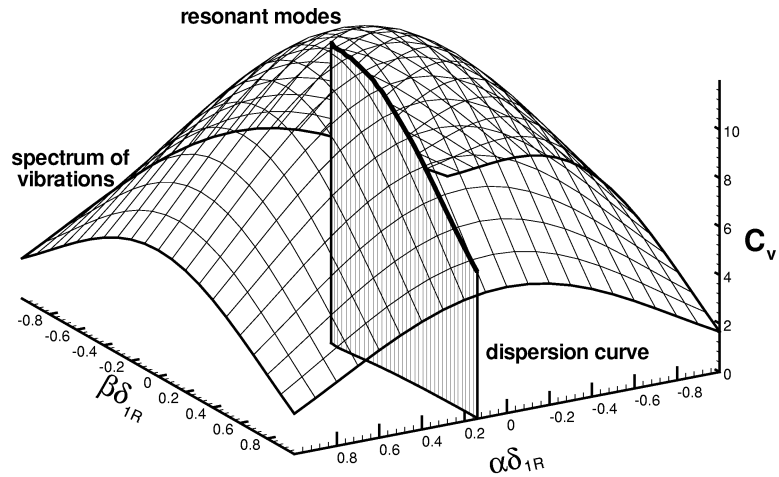

Fig. 18. Amplitude of the wavenumber spectrum of R-source vibrations together with the dispersion curve and the selected resonant modes.

approximated via a least-squares fit by an even polynomial of 8th order. The polynomial coefficients were then used for the calculation the wavenumber spectrum of vibrations discussed in the next section.

7.2. Wavenumber spectrum of vibrations and selection of resonant modes

After having performed a double spatial Fourier transform of the measured shape of the R-source vibrations the 2D wavenumber spectrum of the vibrations was obtained. This spectrum is shown in Fig. 18. Similar to the shape of the vibrations in physical space (x, z) the wavenumber spectrum is axisymmetric in Fourier space (α_R, β). Since the shape of the membrane vibration in physical space is the same in all measurement regimes the 2D wavenumber spectrum of the vibrations shown in Fig. 18 is common for all regime. This spectrum was used for subsequent data processing, namely for the selection of the resonant modes performed with the help of the initial dispersion curves obtained experimentally.

Since the dispersion function $\alpha_R = \alpha_R(\beta)$ for the 3D normal TS waves depends on the disturbance frequency, the Reynolds number, and the streamwise pressure gradient, the resonant spectra of vibrations are different in different measurement regimes. An example of the resonant spectrum of vibrations is shown in Fig. 19 for the FPG case and three frequencies. These spectra were used to determine the receptivity functions.

8. Receptivity functions

When the initial wavenumber spectrum in the boundary layer is determined from the hot-wire measurements and the resonant spectrum of vibrations is obtained, the experimental complex receptivity coefficients can be found for every normal oblique TS-mode as a function of the disturbance frequency and the spanwise wavenumber.

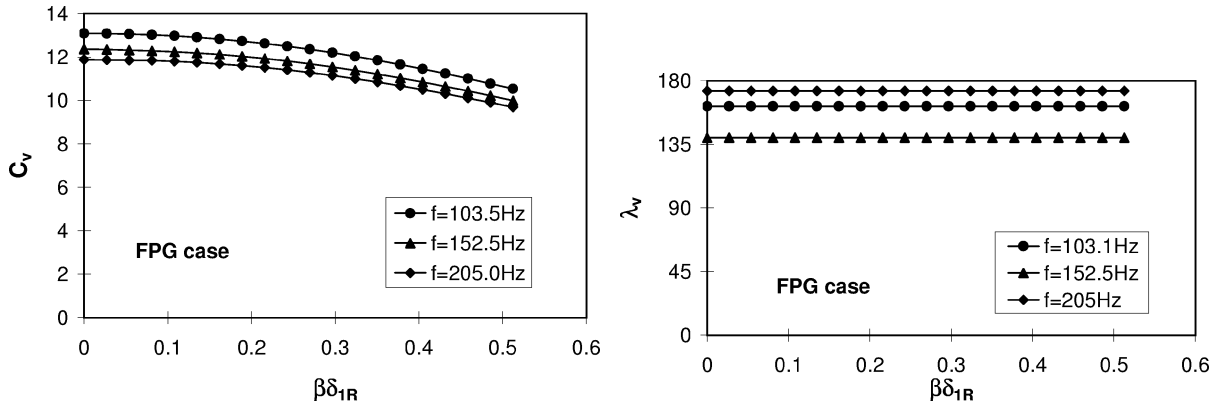

Fig. 19. Amplitude [left] and phase [right] parts of resonant spectra of R-source vibrations measured for FPG case ($Re = 698$).

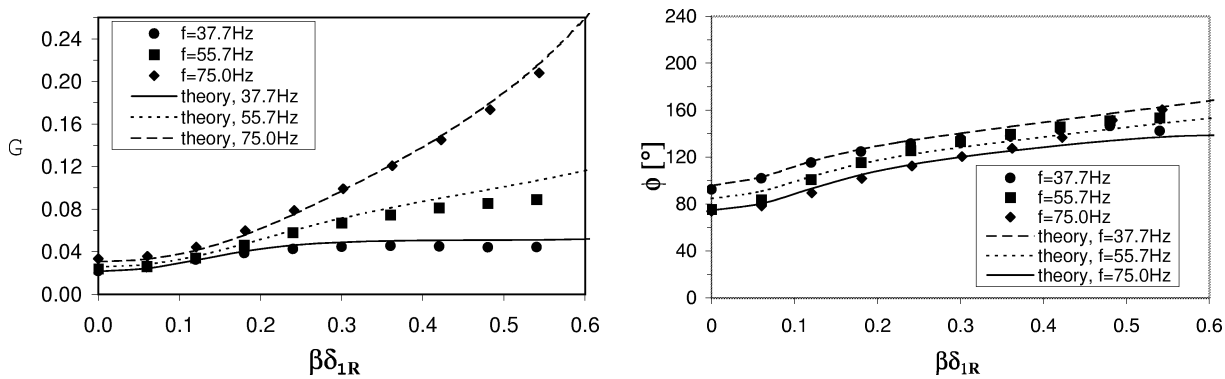

Fig. 20. Amplitude [left] and phase [right] of the complex receptivity coefficients versus spanwise wavenumber measured (symbols) and calculated (curves) in the ZPG case for three frequencies of vibrations ($Re = 946$).

In Fig. 20 the experimentally determined complex receptivity functions are shown in comparison with the calculated ones for the ZPG case. The corresponding results for the FPG case are presented in Fig. 21. The receptivity amplitudes characterize the effectivness of the receptivity mechanism, whereas the receptivity phases indicate a phase delay between the membrane vibration and the generated TS wave.

In general, good quantitative agreement between the experimental and theoretical results was observed. Only in the FPG case the experimental phases show a small (nearly constant) shift of about 20 degrees compared to the theoretical ones. The cause of this shift is not yet clear. The lowest receptivity was found for the 2D waves. This effect gets stronger when the vibration frequency increases. The receptivity phases displayed a rather weak dependence on both frequency and spanwise wavenumber.

The results obtained for the ZPG case are in a good qualitative agreement with previous experiments by Ivanov et al. [13]. However, the quantitative agreement of the receptivity amplitudes with theory is better in the present case than in the paper by Ivanov et al. [17]. Most probably, the agreement is better since the extrapolation procedure of the TS-wave amplitudes to the R-source position was improved.

The results presented in Figs. 20 and 21 indicate that the receptivity coefficients are not influenced by the weak curvature of the wall so that its neglect in the theoretical approach was justified a posteriori. Therefore, it seems reasonable to extend studies of the effect of the pressure gradient on the theoretical side, since this information cannot be extracted from the experimental data in pure form due to the different Reynolds numbers in the ZPG and FPG experiments.

The corresponding theoretical receptivity amplitudes at the same Reynolds number of $Re = 946$ and the same nondimensional frequency parameters F for both ZPG and FPG cases are presented in Fig. 22. These functions were calculated for the true maximum of the TS-wave amplitudes in wall-normal direction, but there are no significant differences compared with the results shown in Figs. 20 and 21 which were obtained at a fixed nondimensional wall distance y/δ_1. It is seen that the favorable pressure gradient enhances the receptivity amplitudes compared to the Blasius case. For the present value of the Hartree parameter ($\beta_H = 0.10$) this effect is rather weak for 2D modes, but it increases with growing spanwise wavenumber. A qualitatively similar result was obtained for $Re = 698$. The observed influence of the pressure gradient is consistent with

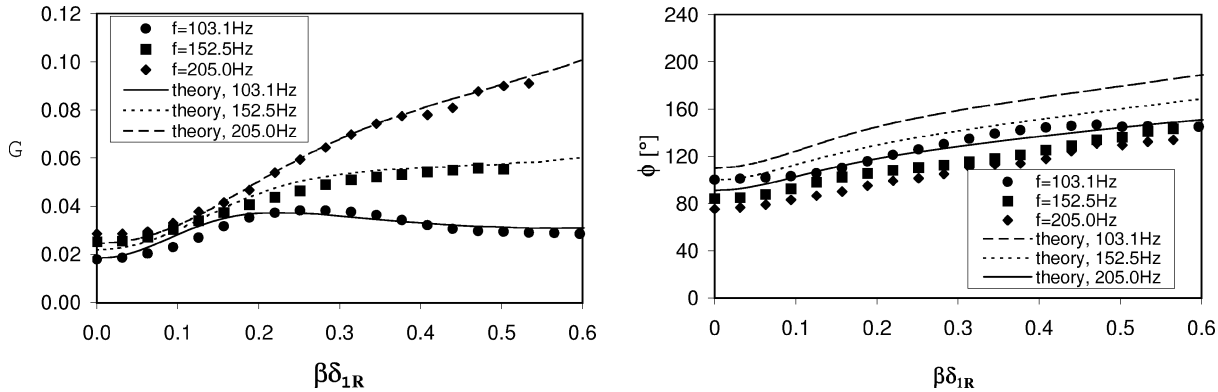

Fig. 21. Amplitude [left] and phase [right] of the complex receptivity coefficients versus spanwise wavenumber measured (symbols) and calculated (curves) in the FPG case for three frequencies of vibrations ($Re = 698$).

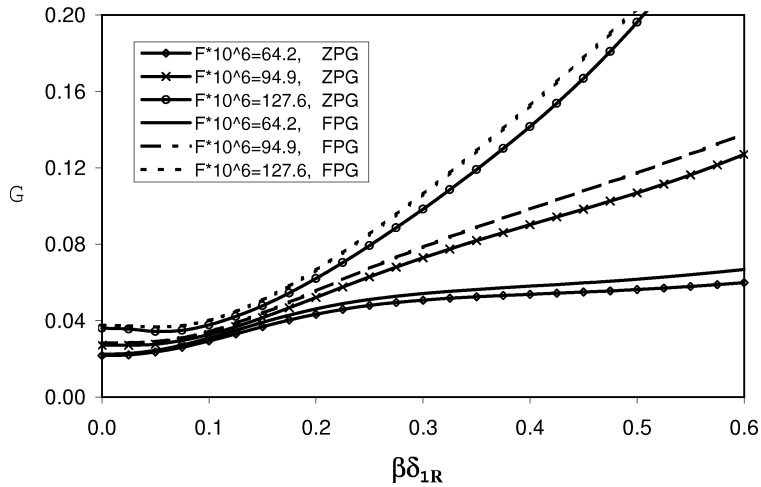

Fig. 22. Receptivity amplitudes versus spanwise wavenumber calculated for $Re = 946$ in the ZPG and FPG case for three frequencies of vibrations.

theoretical results obtained by Michalke and Neemann [16] and Neemann [20] for the boundary-layer receptivity to periodic blowing or suction at the wall.

9. Conclusions

The following conclusions can be drawn from the results of the combined experimental and theoretical study of the 3D linear receptivity of boundary layers to localized surface vibrations performed in two flows: (i) zero streamwise pressure gradient (Blasius flow) and (ii) favorable streamwise pressure gradient with a Hartree parameter $\beta_H = 0.10$.

1. For both boundary-layer flows the values of the complex receptivity coefficients were obtained experimentally and theoretically for various normal oblique TS-modes as functions of the disturbance frequency and the spanwise wavenumber (or the wave propagation angle). These coefficients are independent of the specific shape of the surface vibration since they are defined in the Fourier space for the linear receptivity problem and any specific shape of vibration can be composed of the corresponding frequency-wavenumber modes.

2. Good quantitative agreement between the experimental and theoretical results was found for the receptivity amplitudes (in both basic flows) and the phases in the ZPG boundary layer. In the FPG flow the theoretical receptivity phases were somewhat larger than the experimental ones.

3. It was found that the weak spanwise curvature of the wall (with the ratio of the boundary-layer displacement thickness to the radius of curvature $\delta_1/R \approx 0.008$) does not influence the receptivity amplitudes in the present parameter range since the deviation of the experimental to the theoretical results is within the measurment accuracy.

5. Both boundary layers are shown to be more receptive to 3D perturbations than to 2D ones. The receptivity amplitudes increase with the spanwise wavenumber, the wave propagation angle, and the disturbance frequency, whereas the receptivity phases depend rather weakly on these parameters. For the case of the Blasius boundary layer these results agree with previous experimental observations.

6. The favorable pressure gradient was found to enhance slightly the vibration receptivity amplitudes in the range of parameters studied. This effect increases with growing spanwise wavenumber and agrees with previous theoretical results obtained for the receptivity to periodic blowing or suction at the wall.

One may note in the end, that the physical nature of the vibration receptivity mechanism studied in the present work is very close to that of the boundary-layer receptivity to blowing-suction disturbances (see Neemann [20]) because the v-component of the velocity fluctuations produced at the wall (that is present in the two cases) seems to play the dominant role in both these mechanisms. The roughness receptivity, important in 3D boundary layers, can be also regarded as an extreme case of the vibration receptivity when the frequency of vibrations tends to zero (see, e.g., Kachanov [7]). Therefore, the results obtained in the present work have also a certain importance when considering the other receptivity problems mentioned above.

Acknowledgements

The present research project is part of a cooperation between the Hermann-Föttinger-Institute of Fluiddynamics, TU Berlin (Germany) and the Institute of Theoretical and Applied Mechanics in Novosibirsk (Russia) supported by Deutsche Forschungsgemeinschaft (grant FE 43/42-1) and the Russian Foundation of Basic Research (grant N 98-01-04090).

References

[1] M.V. Morkovin, Critical evaluation of transition from laminar to turbulent shear layer with emphasis of hypersonically travelling bodies, AFFDL Tech. Rep. 68-149, 1968.
[2] M. Gaster, On the generation of spatially growing waves in a boundary layer, J. Fluid Mech. 22 (1965) 433–441.
[3] E. Reshotko, Boundary-layer stability and transition, Annu. Rev. Fluid Mech. 8 (1976) 311–349.
[4] M.V. Morkovin, Instability, transition to turbulence and predictability, AGARD-AG-236, 1977.
[5] Y.S. Kachanov, V.V. Kozlov, V.Y. Levchenko, Beginning of Turbulence in Boundary Layers, Nauka, Novosibirsk, 1982 (in Russian).
[6] M. Nishioka, M.V. Morkovin, Boundary-layer receptivity to unsteady pressure gradients: experiments and overview, J. Fluid Mech. 171 (1986) 219–261.
[7] Y.S. Kachanov, Three-dimensional receptivity of boundary layers, Eur. J. Mech. B/Fluids 19 (5) (2000) 723–744.
[8] E.D. Terentev, The linear problem of a vibrator in a subsonic boundary layer, PMM U.S.S.R. 49 (1981) 791–795.
[9] A.M. Tumin, A.V. Fedorov, Generation of instability waves in a boundary layer on a vibrating surface, Zhurn. Prikl. Mekhan. Tekhn. Fiz. 3 (1983) 72–79 (in Russian).
[10] A.M. Tumin, A.V. Fedorov, Instability wave excitation by a localized vibrator in a boundary layer, J. Appl. Mech. Tech. Phys. 25 (1984) 867–873.
[11] V.M. Gilev, V.V. Kozlov, Excitation of Tollmien–Schlichting waves in the boundary layer on a vibrating surface, J. Appl. Tech. Mech. Phys. 25 (1984) 874–877.
[12] A.V. Ivanov, Y.S. Kachanov, T.G. Obolentseva, Experimental investigation of flat-plate boundary-layer receptivity to 3D surface vibrations, in: Wagner S. (Ed.), Book of Abs., Euromech Coll. 359, Stability and Transition of Boundary-Layer Flows, Inst. Aero- und Gasdynamik, Uni. Stuttgart, 1997, pp. 10–13.
[13] A.V. Ivanov, Y.S. Kachanov, T.G. Obolentseva, Experimental study of Blasius boundary layer receptivity to localized surface vibrations, Thermophysics Aeromechanics 6 (2) (1999) 179–192.
[14] A. Michalke, Receptivity of axisymmetric boundary layers due to excitation by a Dirac point source at the wall, Eur. J. Mech. B/Fluids 14 (1995) 373–393.
[15] A. Michalke, Excitation of a 3D-wavetrain by a Dirac point source at the wall and its growth in a decelerated laminar boundary layer, Eur. J. Mech. B/Fluids 16 (1997) 779–795.
[16] A. Michalke, K. Neemann, Excitation of 3D-disturbances in wall-bounded shear flow with adverse pressure gradient, Acta Mech. 124 (1997) 219–224.
[17] A. Ivanov, Y. Kachanov, T. Obolentseva, A. Michalke, Receptivity of the Blasius-boundary-layer to surface vibrations. Comparison of theory and experiment, in: Int. Conf. on Meth. of Aerophys. Research. Proceedings. Part I (1998), Inst. Theor. Appl. Mech., Novosibirsk, 1998, pp. 93–98.
[18] Y.S. Kachanov, D.B. Koptsev, B.D. Smorodsky, 3D stability and receptivity of two-dimensional self-similar boundary layer with adverse pressure gradient, in: Fasel H., Saric W.S. (Eds.), Laminar-Turbulent Transition (1999), Springer, Berlin, 2000, pp. 571–582.

[19] A. Michalke, K. Neemann, Excitation of instability waves in wall boundary layers with adverse pressure gradients by various types of Dirac sources, Acta Mech. 122 (1997) 33–48.
[20] K. Neemann, Theoretische Untersuchungen zur Anregbarkeit instabiler Wellen in kompressiblen Wandgrenzschichten, PhD thesis, Technical University Berlin, Germany, 1999.
[21] S. Bake, H.H. Fernholz, Y.S. Kachanov, Resemblance of K- and N-regimes of boundary-layer transition at late stages, Eur. J. Mech. B/Fluids 19 (2000) 1–22.
[22] V.M. Gilev, Y.S. Kachanov, V.V. Kozlov, Development of a spatial wave packet in a boundary layer, Izv. Sib. Otd. Akad. Nauk SSSR, Ser. Tekh. Nauk. 13 (3) (1983) 27–37 (in Russian).
[23] Y.S. Kachanov, A. Michalke, Three-dimensional instability of a flat plate boundary layer: Theory and experiment, Eur. J. Mech. B/Fluids 13 (1994) 401–422.
[24] H. Schlichting, Boundary Layer Theory, 7th edn., McGraw-Hill, New York, 1979.
[25] Th.L. van Stijn, A.I. van de Vooren, An accurate method for solving the Orr–Sommerfeld equation, J. Eng. Math. 14 (1980) 17–26.
[26] D.E. Ashpis, E. Reshotko, The vibrating ribbon problem revisited, J. Fluid Mech. 213 (1990) 531–547.
[27] H.H. Fernholz, D. Warnack, The effect of a favorable pressure gradient and of the Reynolds number on an incompressible axisymmetric turbulent boundary layer. Part 1. The turbulent boundary layer, J. Fluid Mech. 359 (1998) 329–356.